DOI:
10.1088/1361-6668/acf739

Document Version
Peer reviewed version

Characterization of Flux Pump-Charging of High-Temperature Superconducting Coils using Coupled Numerical Models

Pengbo Zhou[1,2*], **Asef Ghabeli**[2], **Mark Ainslie**[3] **and Francesco Grilli**[2]

1 State Key Laboratory of Rail Transit Vehicle System, Southwest Jiaotong University, Chengdu, China

2 Institute for Technical Physics, Karlsruhe Institute of Technology, Karlsruhe, Germany

3 Department of Engineering, King's College London, London WC2R 2LS, UK

E-mail: `Pengbo.zhou@kit.edu, chrischouchina@163.com`

Abstract.

Flux pumps provide a promising solution for contactless charging of high-temperature superconducting (HTS) coils, eliminating the need for bulk current leads and reducing the heat burden for the cryogenic system. Characterizing the nonlinear effects of an HTS coil charged by a flux pump and understanding the dynamics of the charging process is essential for promoting the practical application of flux pumps. Numerical models provide a fast and cost-effective way of achieving this. In this study, we propose a methodology for coupling HTS coil and flux pump models using an electrical circuit, resulting in reduced computation costs. We validate the effectiveness of our approach against the experimental results of an HTS coil charged by a dynamo-type flux pump. Specifically, we obtain the voltage produced by the HTS dynamo using a 3D model based on the minimum electromagnetic entropy production (MEMEP) method and apply this voltage to the load HTS coil using a *T-A* formulation finite-element method (FEM) model coupled via an electrical circuit. The simulated charging current shows good agreement with experimental observations, validating our modeling strategy. The results demonstrate that the flux flow state in the HTS coil is the primary factor limiting the charging performance of the HTS dynamo as the charging current approaches the coil's critical current. Furthermore, based on the simulation, we demonstrate that, when using flux pumps, it is advisable to leave a margin between the operating current and the critical current of the coil. Overall, our approach has the potential to be applied to HTS coils charged by any device.

1. Introduction

Flux pumps are a promising technology for applications involving HTS coils, such as MAGLEV and rotors/motors, where maintaining a persistent current mode can be challenging due to dynamic losses. Conventionally, a power supply must remain connected to the HTS coil to maintain the current flowing through HTS coils, and thick current leads are used to transmit the current between cryogenic and ambient environments, resulting in heat losses that limit performance and efficiency. Flux pumps can inject direct current into a closed-loop superconducting circuit without electrical contact, eliminating the need for current leads and reducing heat losses [1–6]. This feature makes them highly suitable for HTS coils. As a result, there has been significant interest in flux pumps, leading to the proposal and testing of numerous types of flux pumps [7–13]. Until now, there are two main categories of flux pumps for HTS coils: the HTS dynamo, which bears similarities to traditional dynamos but operates without the need of commutators or brushes [14–16], and the transformer-rectifier HTS flux pump, which functions much like a typical rectifier except that the HTS bridge serves as the rectifying element [17–19].

To comprehend the working mechanism and facilitate the practical implementations of both the HTS dynamo and the transformer-rectifier-type HTS flux pumps, numerical modeling has become an indispensable tool [20]. Mataira et al. developed an H-formulation-based model to simulate the open-circuit voltage generated by the HTS dynamo and concluded that the non-linear electromagnetic characteristics of HTS materials result in the rectifying effect of the HTS dynamo [21, 22]. A model developed by Ainslie et al. takes into account the real geometry of the HTS tape and shows that the current sharing effect in the HTS tape can lead to performance degradation as the frequency of rotation increases [23]. Using a 2D segregated model, Zhou et al. found that the performance of the HTS dynamo reaches an optimal level for a specific number of permanent magnets [24]. Sokolovsky et al. employed the Chebyshev spectral method to develop a numerical model to investigate the influence of ferromagnetic materials on the performance of the HTS dynamo [25]. Ghabeli et al. developed a 3D model for assessing the HTS dynamo based on the minimum electromagnetic entropy production method (MEMEP) [26]. Geng et al. built a 2D H-formulation to simulate the transformer-rectifier-type HTS flux pump, which is useful for gaining a fundamental understanding of the system, but limited to the practical application due to a number of simplifications [27]. Later, Zhou et al. proposed a model for the self-regulating HTS flux pump, which is able to capture all the critical factors [28].

So far, the majority of numerical studies regarding the HTS flux pumps have concentrated on the open-circuit DC voltage of the HTS dynamo or its behavior with a DC transport current [29]. A few numerical models take into account the load HTS coil. The models from [30] consider the HTS coil as an ideal inductance without taking into account its non-linear properties and dynamic effects. In practical scenarios, where the DC component of the dynamo voltage is crucial, one cannot

overlook the time-varying AC voltage that is actually generated in the dynamo during each cycle of rotation [17, 30, 31]. While this voltage does not directly contribute to the accumulation of DC current in the HTS coil, it induces AC ripples in the charging current waveform [30]. The impact of these AC ripples on the dynamic behavior of the HTS coil during the charging process needs further investigation. Moreover, the critical current of the HTS coil plays a crucial role in the charging process as it limits the value of the saturated current, as reported in experiments [32, 33]. Overall, the development of a numerical model that can include the dynamic effects of the HTS coil is crucial for a more comprehensive understanding of the behavior of the system.

In the present investigation, we propose a modeling approach that considers the limitations imposed by the critical current of the HTS coil during charging and the computation of AC losses in the HTS coil. This approach involves simulating the behavior of the HTS coil independently while obtaining the input for the HTS coil model from another model. Based on the HTS coil charging experiment reported by Jiang et al. [32, 33], we validate our modeling strategy. Specifically, the voltage generated by the HTS dynamo is simulated using a model based on the 3D minimum electromagnetic entropy production method (3D MEMEP) method, and the behavior of the load HTS coil is modeled using a *T-A* formulation-based method. The proposed modeling framework allows for the analysis of the dynamic behavior of the HTS coil during the charging process, including the voltage generated and the AC loss. In addition, the behavior of the HTS coil after switching off the flux pump is investigated using this model.

2. Problem Configuration

The experimental set-up and data are from [32, 33]. For the reader's convenience, here below we report a brief description of the system and of the experimental conditions. Figure 1 shows the configuration of the studied problem. The whole system can be separated into two main parts: (a) the HTS dynamo containing the rotating permanent magnets and the HTS stator, and (b) the load HTS coil connected to the HTS stator. With the rotation of the permanent magnets transiting past the HTS stator, a net DC voltage is generated due to the non-linear *E-J* relation of the HTS materials [21, 34]. During this process, the current is consequently injected into the load HTS coil. In this regard, the experiment reported in [32,33] detailed a permanent magnet rotor comprised of two circular wheels. The central distance between the two discs (with a radius of 35 mm) is 17.5 mm, each of them containing 12 cylindrical N38 NdFeB magnets, which are equally distributed around the circumference. The magnets have a height of 10 mm and a radius of 5 mm. The HTS stator, which is made of stabilizer-free SuperPower tape (SF12100-CF), has a width of 12 mm and a self-field critical current of 313 A. The gap between the surface of the magnets and the HTS stator, known as the flux gap, varies from 1.0 to 7.5 mm. The rotational frequency ranges from 4 Hz to 50 Hz, corresponding to an operating frequency of 48 Hz to 600 Hz (because each rotor contains 12 magnets).

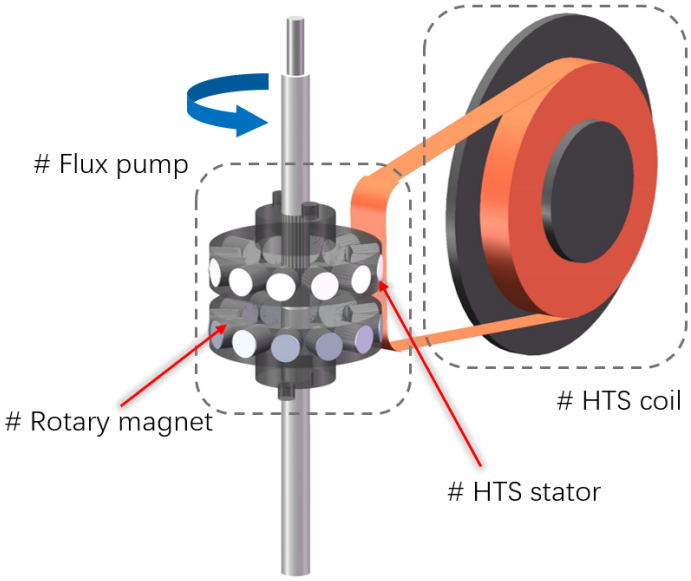

Figure 1. Configuration of the HTS coil charged by dynamo-type flux pump as reported in the experiments by Jiang et al. in [32, 33].

The HTS stator is soldered to a double pancake coil wound with 4 mm-wide AMSC coated conductor, which spans a total length of 40 m and exhibits a self-field critical current of 88 A. The double pancake coil comprising 163 turns with inner and outer diameters of 50 mm and 90 mm, respectively, was characterized at 77 K. Its inductance and self-field critical current were measured to be 2.4 mH and 55 A, respectively.

Based on the experimental results, when the HTS dynamo is operated at a frequency of 600 Hz and a 1 mm flux gap, the injected transport current in the HTS coil could reach 58 A, exceeding its critical current of 55 A. This indicates the presence of a resistive voltage in the HTS coil, which in turn limits the overall performance of the HTS dynamo. The corresponding voltage measurements (see Figures 4 and 5 in [33]) provide clear evidence of this effect. In other operating cases, the transport current is lower, and the impact from the HTS coil is not that significant. As a result, in this study, we focus primarily on investigating the performance of the HTS coil under the aforementioned conditions. A summary of the relevant parameters is provided in Table 1.

3. Modelling Strategy

Simulating the entire coupled system accurately within one model would require a comprehensive and complicated 3D modeling approach to incorporate all components (HTS dynamo rotor and stator and load HTS coil). This presents significant challenges, including the computational resources required. To address this issue, we propose a methodology that models the HTS dynamo and HTS coil separately, coupling these two

Table 1. Modelled system parameters

Rotor	Radius	35 mm
	Central distance between discs	17.5 mm
Permanent magnet (N38 NdFeB)	Number	24
	Radius	5 mm
	Height	10 mm
	Remanent flux density	1.25 T
HTS stator (SuperPower SF12100-CF)	Width	12 mm
	Critical current (self-field)	313 A
HTS coil (AMSC)	Tape width	4 mm
	Tape critical current (self-field)	88 A
	Pancakes	2
	Total turns	163
	Coil inner diameter	50 mm
	Coil outer diameter	90 mm
	Coil critical current	55 A
	Self-inductance	2.4 mH
Operating parameters	Operating frequency	48, 192, 600 Hz
	Flux gap	1 mm

models via an electrical circuit. According to previous literature [8], as shown in figure 2, the HTS dynamo can be characterized as a DC voltage source V_{OC} connected in series with a resistor R_d, and the HTS coil is represented as an inductor L_{HTS} connected in series with a resistor R_{HTS}. Based on the arrangement depicted in figure 1, the magnetic field produced by the HTS coil around the HTS stator primarily aligns parallel to its surface, having a limited influence on the stator's electromagnetic performance. Moreover, the magnetic field generated by the permanent magnets decays dramatically with distance, usually following a $1/r^3$ relationship (where r represents the distance) [34], having a negligible impact on the HTS coil. As a result, the interaction between the two components' magnetic fields can be disregarded, enabling independent FEM modeling of these two parts. Accordingly, we separate the modeling process into two models: the first model simulates the magnetization of the HTS stator carrying DC transport current, and the second model simulates the charging of the HTS coil via a voltage source. The voltage output from the first model is used as the input for the second model. It is worth noting that in order to accurately model the dynamic behavior of the HTS coil, an instantaneous voltage $V_{OC}(t)$ is needed [30].

In this study, the first model is built by using the 3D MEMEP approach [26] to obtain the precise instantaneous voltage generated by the HTS dynamo. The resistor R_d is set to be a constant value of 1.2 mΩ determined by the measurement [33], which can also be obtained by simulation [30]. Considering that this resistor is more than

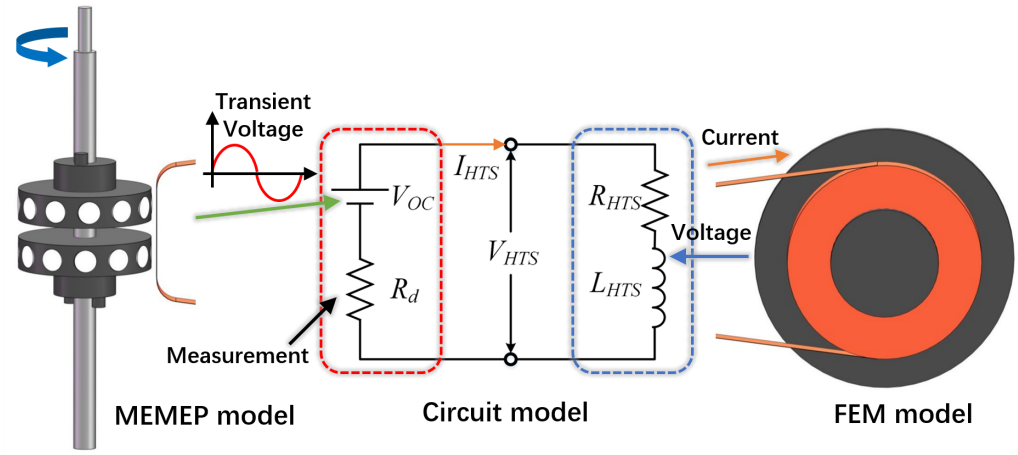

Figure 2. Illustration of the modeling strategy, wherein the MEMEP model calculates the transient voltage, which is subsequently applied to the HTS coil simulated by another FEM model.

1000 times larger than the joint resistance of 0.88 $\mu\Omega$, we neglect the contribution of the joint resistance in the calculations. As for the second model, we adopt the modeling strategy proposed in [35–37]. This approach enables us to evaluate the overall behavior of superconducting systems that involve various power components while maintaining a high level of precision regarding the local superconducting effects. The strategy involves coupling the electrical circuit model with the numerical model by representing the HTS components as a voltage drop V_{HTS} in the circuit. This voltage is given by the integration of the electrical field and magnetic vector potential along the superconducting path. The resulting current I_{HTS} calculated by the circuit is then fed back into the HTS coil numerical model to achieve the coupled simulation.

3.1. MEMEP 3D for the HTS dynamo

The MEMEP 3D method is a variational method based on the **T**-formulation, which obtains the solution of the problem by minimizing the entropy production generated by the electromagnetic fields [38, 39]. MEMEP 3D solves the problem by minimizing a functional containing variables including the magnetic vector potential, **A**, and effective magnetization, **T**, where $\nabla \times \mathbf{T} = \mathbf{J}$. It was proven that the minimum of this functional in the quasi-magnetostatic limit is the only solution of Maxwell's differential equations [39]. The 3D functional as a function of **T** as the only variable is:

$$L = \int_V dv[\frac{1}{2}\frac{\Delta \mathbf{A}_J}{\Delta t} \cdot (\nabla \times \Delta \mathbf{T}) + \frac{\Delta \mathbf{A}_M}{\Delta t} \cdot (\nabla \times \Delta \mathbf{T}) + U(\nabla \times \mathbf{T})], \qquad (1)$$

where V is the volume of the sample, $\mathbf{A}_M$ and $\mathbf{A}_J$ are two known variables, the vector potential due to the applied field (in the case of the HTS dynamo due to a

magnet or several magnets) and the vector potential due to the current density in the superconductor, respectively. $\mathbf{A}_J$ can be easily calculated with the volume integral of current density and $\mathbf{A}_M$ is calculated analytically [26]. U is the dissipation factor, defined as [39]

$$U(\mathbf{J}) = \int_0^{\mathbf{J}} \mathbf{E}(\mathbf{J}') \cdot d\mathbf{J}'. \tag{2}$$

This dissipation factor can include any E-J relation for superconductors or normal conductors. In our problem, we have used an isotropic E-J power law to describe the non-linear resistivity of the HTS material as

$$\mathbf{E}(\mathbf{J}) = E_c \left(\frac{|\mathbf{J}|}{J_c} \right)^n \frac{\mathbf{J}}{|\mathbf{J}|}, \tag{3}$$

where $E_c = 10^{-4}$ V/m is the critical electric field, J_c is the critical current density and n is the n-value of the superconducting material. Both J_c and n depend on the magnitude and direction of the magnetic field.

To model the 24 cylindrical permanent magnets (rotating in the xz-plane, see Figure 1) and obtain the resultant $\mathbf{A}_M$ to be replaced in the functional, the procedure is very similar as explained for a single cylindrical magnet in [26].

The vector potential and magnetic field at certain observation points inside the tape are calculated analytically for each magnet and then superimposed together to obtain the total value for the 24 magnets.

The $I_c(B, \theta)$ and $n(B, \theta)$ characteristics of the HTS tape (see Figure 3, and Table 1) were both implemented in the model and used by interpolating the experimental points. The data were measured and provided by the Robinson Research Institute, Victoria University of Wellington in New Zealand, using their SuperCurrent facility [40]. In the HTS tape model (x-axis along the thickness and y-axis along the length) only the superconducting layer with 1 μm thickness has been modeled and the tape length was chosen to be 76 mm, which is considered to be enough to calculate the output voltage in the flux pump.

For the HTS tape with the dimensions of 12 mm×76 mm×1 μm in the x, y, z directions, respectively, we have chosen 51×201×1 mesh elements. We have demonstrated previously in [26, 30, 34] that for similar flux pump modeling, only one element along the thickness of the tape suffices. We have also investigated that with increasing the element number in the x and y directions, the change in the output result is negligible. With a total number of 10,251 elements and using a computer with the specification of an AMD Ryzen Threadripper 3970x 32-core processor and 128 GB RAM and Ubuntu 20.04.4 LTS operating system, the calculation time for flux gap of 1 mm and 2 cycles is 25 hours and 20 minutes. Note that the simulation has been performed only in 30° of magnets' rotation out of 360° due to symmetry.

The output instantaneous open-circuit voltage of the stator is calculated as

$$V_{OC}(t) = \frac{1}{w} \int_{-\frac{w}{2}}^{+\frac{w}{2}} dx \int_{-\frac{l}{2}}^{+\frac{l}{2}} dy \left[\partial_t A_y + E_y \right], \tag{4}$$

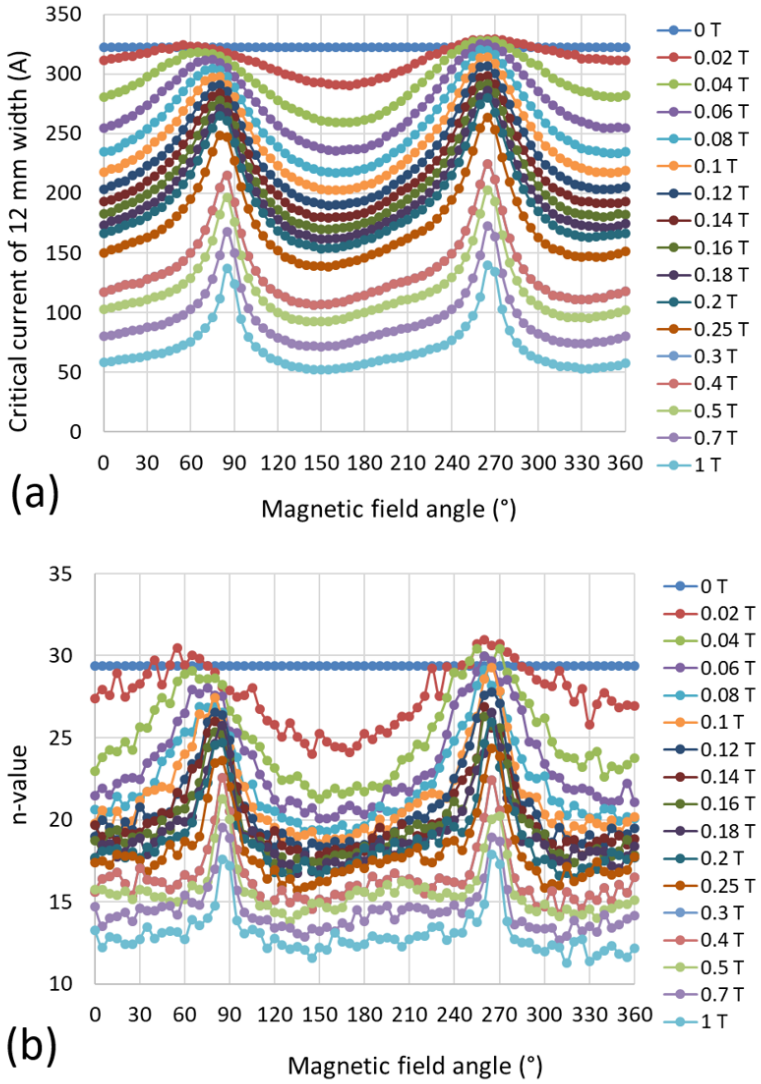

Figure 3. Measured $I_c(B,\theta)$ and $n(B,\theta)$ data at 77 K for the SuperPower tape (SF12100-CF), implemented in the HTS stator model of the flux pump. θ is the angle of the applied magnetic field with respect to the normal vector of the tape surface.

where l is the length and w is the width of the tape, and A_y and E_y are the y components of the total vector potential and electric field, respectively. The DC value of the instantaneous open-circuit voltage can be calculated as

$$V_{DC} = f \int_0^{1/f} V_{OC}(t)\, dt, \tag{5}$$

where f is the rotational frequency of each magnet passing across the HTS tape. This value is an important parameter for showing the efficiency of a flux pump and the higher the value of V_{DC} is, the better the pumping performance of a flux pump.

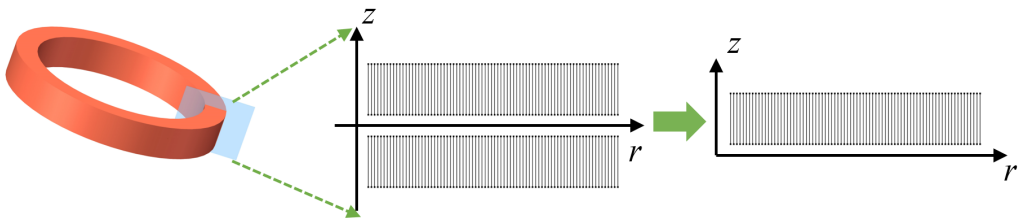

Figure 4. The cross-sectional geometry of the double pancake HTS coil model. Due to the symmetry, only the top pancake is actually simulated

3.2. Coupled numerical model of the HTS coil

The HTS coil is modeled using the 2D axisymmetric T-A formulation. For more details of this approach, we refer the reader to [41, 42]. Figure 4 shows the cross-sectional geometry. This model only considers the superconducting layers within the HTS tapes. Due to the symmetry, only half of the HTS coil is considered, leading to the simulation of a single pancake. Coupling the HTS coil model with the voltage source and the internal resistance (see Figure 2) is achieved by considering the HTS coil as a voltage drop in the circuit. The voltage of each turn is obtained by the integration of the E_{phi} and $\partial_t A_{phi}$ along the superconducting path:

$$V_{HTS,k} = \left(-\frac{d}{dt} \left[\frac{\int_{w_{tape}} A_{phi} dz}{\int_{w_{tape}} dz} \right] - \frac{\int_{w_{tape}} E_{phi} dz}{\int_{w_{tape}} dz} \right) l_{HTS,k}, \tag{6}$$

where E_{phi} and A_{phi} are the angular components of the electrical field and the magnetic vector potential, respectively, w_{tape} denotes the width of the HTS tape, $l_{HTS,k}$ represents the length of the k^{th} turn, which is equal to $2\pi r_k$, and r_k is the radius of the k^{th} turn. The total voltage developed by the HTS coil is given by summing the voltages of each turn:

$$V_{HTS} = \sum_{k=1}^{N} V_{HTS,k}. \tag{7}$$

The current obtained by the circuit model is then applied to the HTS coil by using a Dirichlet boundary condition.

According to the experiment [33], it takes tens of seconds for the system to reach saturation during the charging process. Given the 600 Hz frequency of the applied voltage, it follows that over 10000 cycles should be computed. To improve the computation speed, a homogenization method is utilized [43, 44]. As we stated in our previous study [45], an auxiliary model including all the turns is needed for accurately simulating the voltage of each turn. The electrical field $\mathbf{E}$ and magnetic field vector potential $\mathbf{A}$ calculated with the homogenized model are mapped to the auxiliary model. The voltage drop calculated by the auxiliary model is applied to the circuit, while the current obtained from the circuit is imposed back into the homogenized model. Figure 5

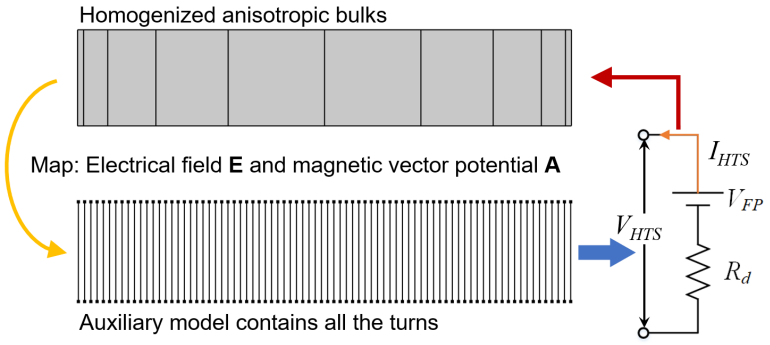

Figure 5. The operation process of coupling the homogeneous method with the electrical circuit.

illustrates the entire process. Our study demonstrated that this approach can be ten times faster compared to the original approach (modeling individual turns) without compromising accuracy [45].

It is worth noting that, by using the given parameters from the experiment [32,33], the inner and outer diameter of 50 mm and 90 mm for the HTS coil, the derived total length and the self-inductance obtained by the model are 36 m and 2 mH, respectively. These values are both smaller than the experimental values of 40 m and 2.4 mH. To align with the reported measurements, we have adjusted the inner and outer diameters of the HTS coil to 57 mm and 97 mm, respectively. This alteration results in a total length of 40 m and a self-inductance of 2.39 mH.

The non-linear resistivity of the superconductor is modeled by the E-J power law in equation (3). A constant value of $n = 21$ is utilized in this model. The field-dependent critical current is described by a Kim-like model:

$$J_c(\mathbf{B}) = \frac{J_{c0}}{(1 + \sqrt{k^2 B_{\parallel}^2 + B_{\perp}^2}/B_0)^{\alpha}}, \tag{8}$$

where $B_{\parallel}$ and $B_{\perp}$ are the parallel and perpendicular components of the magnetic flux density with respect to the surface of the tape, respectively and J_{c0}, B_0, k, and α are material-related parameters. To fit the measured HTS coil self-field critical current of 55 A, these values are set to be 2.2×10^{10} Am^{-2}, 0.085 T, 0.6, 0.25, respectively. The model was implemented using COMSOL Multiphysics 6.0, which led to a calculation time of 12 hours.

4. Results and Discussion

4.1. HTS dynamo modeling results

First, we present the results for a flux gap of 1 mm and an operating frequency of 600 Hz. All the presented results correspond to the second cycle to avoid the transient

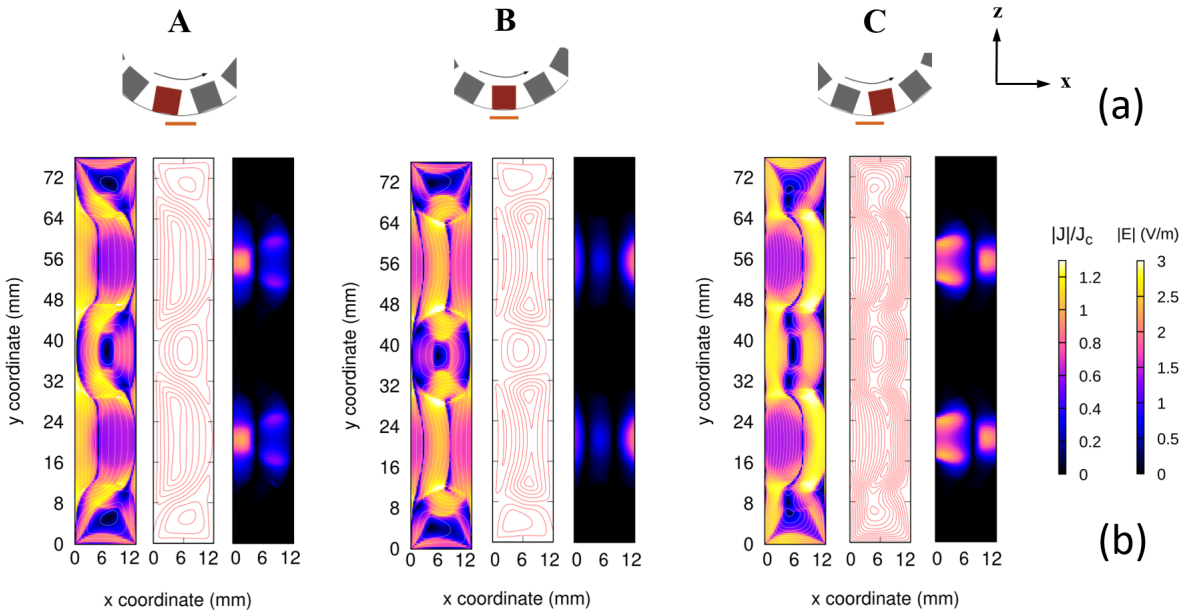

Figure 6. (a) Schematic of the magnets transiting past above the HTS tape for three-time steps corresponding to **A** (260°), **B** (270°) and **C** (280°). At 270° the highlighted magnet is aligned with the center of the tape. Note that there are two 12-magnet discs located along the y direction. (b) Current modulus maps (left side), the corresponding current lines (middle), and electric field modulus maps (right side) in the stator for the three-time steps.

conditions in the tape during the first cycle. Figure 6(b) displays the current modulus maps and current lines along with the electric field maps for three key magnet positions (see Figure 6(a)) including when the highlighted magnets approach the tape at 260° (**A**), when the highlighted magnets are just on top of the tape at 270° (**B**), and when the highlighted magnets move away from the tape at 280° (**C**). The two shadows of the highlighted magnets in purple color indicate that the centers of the two magnets along the y-axis are located at 20.5 mm and 55.5 mm. Two main flows of circulating currents are formed around the two magnets having the most significant impact on the generation of the electric field inside the tape, as can be observed clearly in the electric field maps. Other than that, there are three other circulating currents at the top, bottom, and also between the two central magnets along the y-axis, having a negligible impact on voltage generation in the stator. When the highlighted magnet is just above the tape, the voltage generation is minimal, while when the highlighted magnet approaches or moves away from the tape the voltage generation is maximal. This is in agreement with Figure 8, showing E_{av} that is the net voltage generated by the non-linear resistivity of the HTS tape. Indeed, E_{av} is the volume-average of the electric field equal to the second term in Equation (4).

The distance between the two discs along the y direction should be far enough such

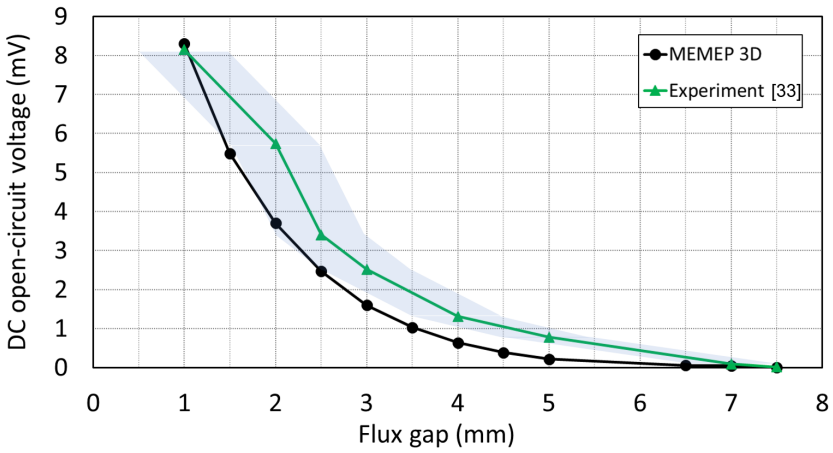

Figure 7. Comparison of the DC open-circuit voltage values obtained from the results of 3D MEMEP modeling and the experiments performed in [33] for different flux gaps from 1 to 7.5 mm. The blue shadow around the experimental results shows the possible error in the results considering ±0.5 mm error in measuring the flux gap.

that the resultant circulating currents due to the two magnets do not interfere with each other, otherwise, there would be an adverse effect on the performance of the flux pump. This can be figured out either by experiment or 3D modeling, but it is impossible with 2D (or 1D) modeling.

Figure 7 shows the calculated MEMEP 3D results for various flux gaps in the range from 1 mm to 7.5 mm in comparison with the results of experiments carried out in [33] (identical flux pump as [32]). The modeling results follow the trend of the experimental results well. The blue shadow around the experimental results shows the possible error considering ±0.5 mm error in measuring the flux gap. This error can arise from the difficulty in precisely measuring the flux gap. It is attributed to the mechanical instability of the flux pump when submerged in the liquid nitrogen bath, as well as the contraction of its constituent parts in the cryogenic environment. Taking into consideration of the flux gap error, the modeling results fit into the blue shadow up to a 2.5 mm flux gap. However, we should not neglect the error of measuring very low values of voltage (around 1 mV) in flux gaps of less than 2.5 mm. This can justify the difference between the modeling results and experiments in a higher flux gap.

4.2. HTS coil modeling results

This section involves the estimation and discussion of various aspects related to the HTS coil. Specifically, we analyze the instantaneous output voltage components, the dynamic charging current curve of the HTS coil, the resulting HTS resistive voltage, and the accompanying AC loss of the HTS coil. In addition, we investigate the dynamic behavior of the current in the HTS coil after switching off the dynamo.

Figure 8 shows the voltages calculated by the MEMEP 3D model for two cycles in

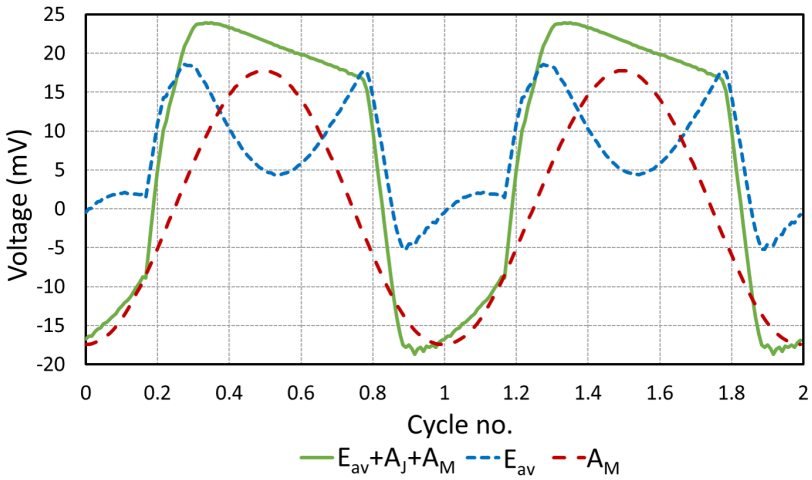

Figure 8. Calculated total output voltage ($[\partial_t A_y + E_y$), resistive voltage (E_y), and inductive voltage ($\partial_t \mathbf{A}_M$) of the HTS dynamo over two cycles by the MEMEP 3D model. This case corresponds to the 1 mm flux gap and 600 Hz operating frequency.

the case of a 1 mm flux gap and a frequency of 600 Hz. There are three distinct voltage components shown, namely the total output voltage $V_{OC}(t)$ obtained by equation (4), the resistive voltage $V_r(t)$ calculated by the integration of E_y, and the inductive voltage $V_i(t)$ calculated by the integration of $\partial_t \mathbf{A}_M$. The inductive voltage produced by the permanent magnets follows a sinusoidal curve. The symmetry of the inductive voltage indicates that it cannot contribute to the accumulation of DC current in the HTS coil. On the contrary, the resistive voltage produced by the superconductor is responsible for the DC current accumulation.

Figure 9(a) shows the simulated charging current curve obtained by applying the total output voltage $V_{OC}(t)$ to the HTS coil alongside the experimental curve for comparison. In addition, the plotted graph also presents the ideal coil current, calculated using the electrical circuit model that simplifies the HTS coil as a lumped inductance parameter as described in [30]. There exists a small discrepancy of approximately 4 A between the measured current saturation value and the simulated current. This is likely attributed to measurement errors of the critical current or transport current of the coil, which will be explored in detail in the following section. Even with the observed discrepancy, the overall comparison between the experimental and simulated results shows excellent agreement, validating our modeling strategy. In contrast, there is a noticeable difference between the analytical current and the measured results. This is because the analytical result ignores the resistive voltage generated by the HTS coil, underscoring the importance of taking into account the critical current limitation of the HTS coil. Figures 9(b)-(d) present the charging current waveforms for several cycles and for different charging stages: at the beginning; when the charging current has increased significantly, and when the charging current saturates. Similar to the findings of Ghabeli et al. [26], the charging current in each cycle exhibits ripples

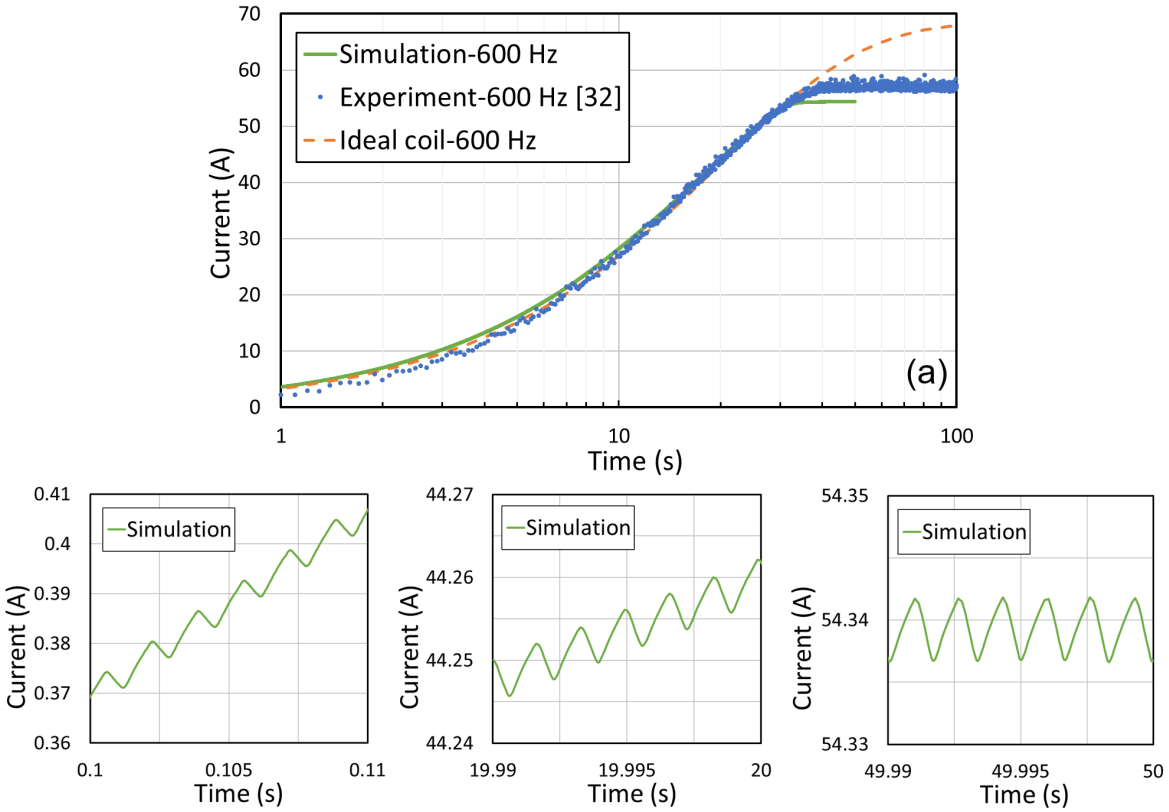

Figure 9. Results of (a) calculated, measured coil current, and ideal coil current, along with detailed waveforms of the calculated charging current at various charging stages: (b) at the initial stage, (c) during the charging current increase and (d) at the point of current saturation. The case corresponds to the 1 mm flux gap and 600 Hz operating frequency. The measured data was obtained from [32].

that are attributed to the inductive voltage. To further verify our modeling approach, we present a similar comparison for the operating frequencies of 48 Hz and 192 Hz in figure 10. The simulated results exhibit a relatively good agreement with the measured results, although there is an earlier discrepancy observed compared to the 600 Hz case (as indicated by the arrows in figure 10). This is likely due to imprecision in the measurement of the dynamic resistance, which decreases proportionally at lower frequencies [32], resulting in less precise measurements. Nonetheless, when comparing the analytical current to the measured one, a different trend is observed. This is due to the ignoring of the resistive voltage generated by the HTS coil, highlighting again the importance of taking into account the limitation imposed by the coil's critical current.

Figure 11(a) shows the resistive voltage of the HTS coil under the case of a 1 mm flux gap and 600 Hz, with its detailed waveform shown in the inset. The voltage curve shows an initial gradual increase as the charging process begins, hinting that the HTS material is in the flux creep state. As the charging continues, the voltage increases at a faster rate until it reaches its peak value, indicating the HTS material is in the flux

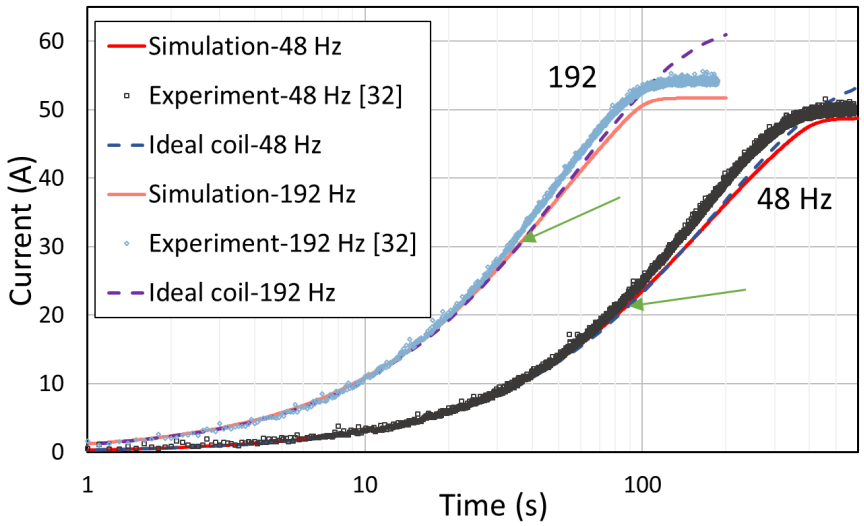

Figure 10. Calculated, measured coil current, and ideal coil current for operating frequencies of 48 Hz and 192 Hz, under the condition of the 1 mm flux gap. The measured data was obtained from [32].

flow state. After reaching the peak, the voltage starts to oscillate around a certain value due to the ripple of the current. The simulated saturated voltage is around 2.1 mV, while the measured saturated voltage is about 1.2 mV, displaying a quite large difference. Here, we attribute the difference to either inaccurate measurement of the critical current, transport current, or resistive voltage in the coil. According to the experiment, the saturated charging current is around 58 A, exceeding the measured critical current of the HTS coil, which is 55 A. Considering the total length of the coil as 40 m, and using the electric field criterion of 1×10^{-4} V/m, the resulting voltage should exceed 4 mV. There are several possible reasons that may have contributed to the unexpected measured results: 1) The critical current of the HTS coil may be higher than the measured value of 55 A, then the measured voltage is lower than the simulated counterpart; 2) The measured saturated current may be less than the actual value of 58 A, leading to a lower measured voltage; 3) The measured saturated voltage may actually be larger than the reported value of 1.2 mV, indicating a potential error in the voltage measurement.

The AC loss generated by the HTS coil during the charging process under the case of 600 Hz is shown in figure 11(b), the inset depicts the detailed waveform of the AC loss when the charging current saturates. The behavior of the AC loss shows the same trend as the HTS resistive voltage. The AC loss exhibits an initial gradual increase at the beginning of the charging process, indicating the presence of hysteresis loss within the superconductor. As the charging process continues, the AC loss accelerates until it reaches its peak value, suggesting the onset of flux flow loss. After reaching its peak value, the AC loss begins to oscillate around a certain value due to the ripple of the current.

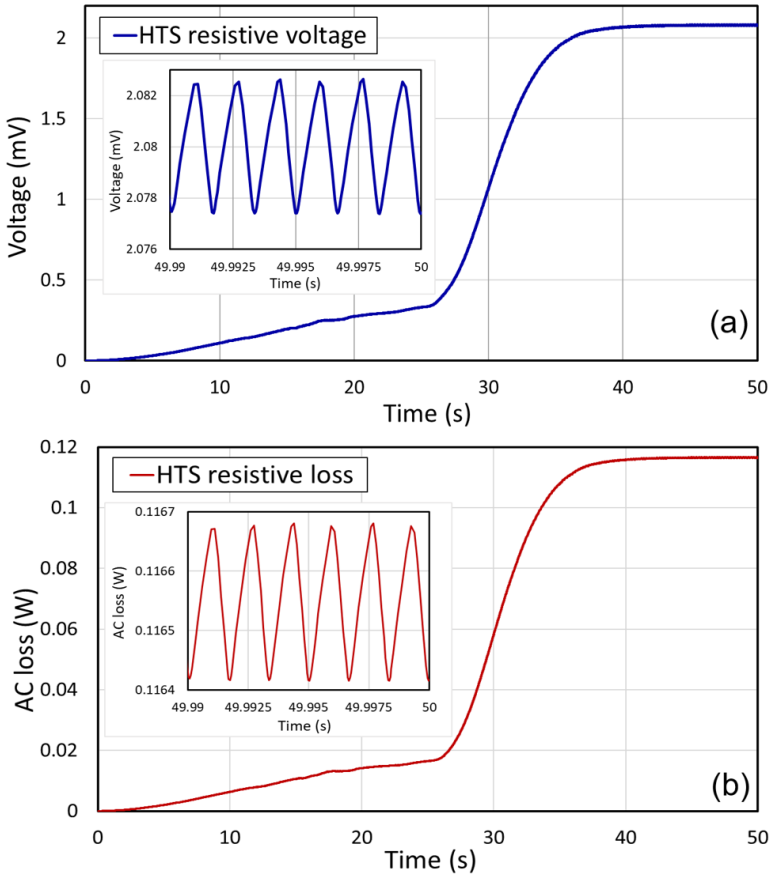

Figure 11. (a) The calculated resistive voltage of the load HTS coil in the whole charging process. The inset shows the detailed waveform of the HTS resistive voltage when the current saturates. (b) The calculated AC loss of the HTS coil during the entire charging process. The inset shows the detailed waveform of the AC loss when the charging current saturates.

According to these results, the HTS coil exhibits both a resistive voltage and AC loss during operation, and in both cases, they enter the flux flow state when the current approaches the critical current of the coil. It is easy to envision that when the flux pump is turned off in a situation when the current is close to the critical current of the coil, the resistive voltage dissipates the energy stored in the coil, resulting in a rapid decline in the current flowing through the HTS coil. We have also performed calculations to study such behavior of the HTS coil in more detail, i.e. when the rotation of the permanent magnets on the rotor of the HTS dynamo is stopped. As shown in figure 12, when the flux pump is switched off and the current is lower than 90 percent of the critical current of the coil, the current continues to flow with (very) little decay. However, if the flux pump is switched off when the current is close to or reaches the critical current of the HTS coil, the current rapidly decreases and saturates around a certain value. As an example, at about 10 % less than the critical current of the coil this current value is approximately 48 A. This suggests that a margin for the operating current should be

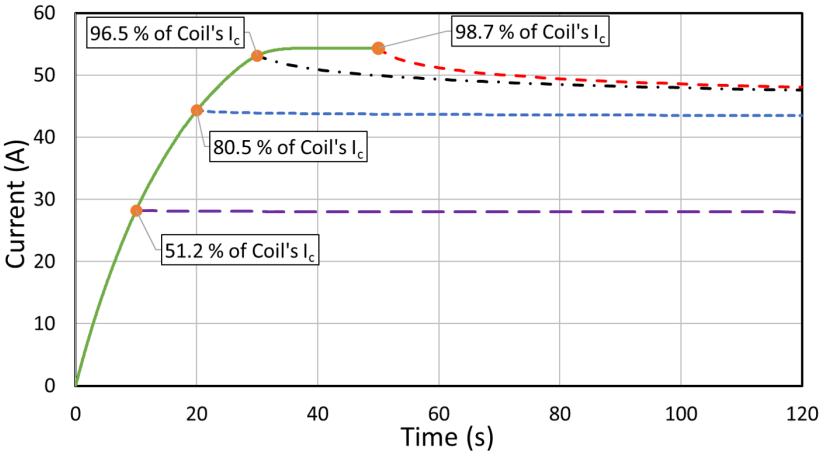

Figure 12. Calculated transport current in the HTS coil (dashed lines) after switching off the HTS dynamo at various times at 10 s, 20 s, 30, and 50 s. The corresponding current levels are 51.2 %, 80.5 %, 96.5 % and 98.7 % of the coil's critical current respectively. The case belongs to the 1 mm flux gap and 600 Hz operating frequency.

considered when charging the HTS coil using such a flux pump, so that the current and hence magnetic field from the coil maintains a near-constant value.

5. Conclusion

To facilitate the practical use of flux pumps, it is crucial to understand the nonlinear effects of the HTS coil during charging by such devices and their combined impact on the dynamics of the charging process. To accomplish this numerically in an efficient manner, we have proposed a methodology that separates the modeling of the HTS coils and flux pumps, reducing computational complexity. The main approach is to first simulate the output voltage of the flux pump and then use it as the input for the modeling of the HTS coil charging process. Our modeling strategy has been validated against measurement results of an HTS coil charged by an HTS dynamo, which involves the use of two circular wheels with a total of 24 circular permanent magnets and a double pancake HTS coil consisting of 163 turns. We have accurately modeled the output voltage of the HTS dynamo using a 3D MEMEP model, which includes both resistive and inductive components. The computational results show excellent agreement with the experimental data. The charging process of the HTS coil is modeled using the *T-A* formulation coupled with an electrical circuit, and a homogenized approach is used to improve computational efficiency. The comparison between the calculated and measured charging current curves shows excellent agreement, with a slight discrepancy in the saturation value of the charging current. This small difference could be attributed to measurement errors. This result validates the effectiveness of our modeling strategy. Simulation results of the HTS coil's voltage and AC loss indicate that as the charging process proceeds, both the voltage and the loss increase gradually. As the current

approaches the critical current of the coil, both the voltage and loss transition into the flux flow state, leading to a rapid rise that restricts the charging performance of the system. Furthermore, the computed coil current after turning off the flux pump at different stages indicates that the voltage and loss due to flux flow can dissipate the energy stored in the coil, leading to a decrease in the current flowing through the HTS coil. In conclusion, our modeling approach enables the evaluation of the performance of the HTS coil charged by a flux pump, which is beneficial for the practical implementation of such flux pumps and their design and optimization.

Acknowledgment

This work was supported in part by the National Natural Science Foundation of China under Grant 52107010, in part by the International Postdoctoral Exchange Fellowship Program between Helmholtz and OCPC, in part by the Natural Science Foundation of Sichuan Province under Grant 2022NSFSC1891, and in part by the Research Funds of State Key Laboratory of Rail Transit Vehicle System under Grant 2022TPL-T11. The authors kindly thank Andres E. Pantoja (Robinson Research Institute, Victoria University of Wellington) for the $I_c(B, \theta)$ and $n(B, \theta)$ measurements of the HTS tape and Zhenan Jiang (from the same institution) for useful discussions about experimental measurements..

References

[1] Klundert V and Kate T. Fully superconducting rectifiers and flux pumps part 1: Realized methods for pumping flux. *Cryogenics*, 21(4):195–206, 1981.

[2] Klundert V and Kate T. On fully superconducting rectifiers and flux pumps. a review. part 2: Commutation modes, characteristics and switches. *Cryogenics*, 21(5):267–277, 1981.

[3] Coombs T A, Geng J, Fu L and Matsuda K. An overview of flux pumps for HTS coils. *IEEE Trans. Appl. Supercond.*, 27(4):1–6, 2016.

[4] Coombs T A. Superconducting flux pumps. *J. Appl. Phys.*, 125(23):230902, 2019.

[5] Wen Z, Zhang H and Mueller M. High temperature superconducting flux pumps for contactless energization. *Crystals*, 12(6):766, 2022.

[6] Wang W, Wei J, Yang C, Wu C and Li H. Review of high temperature superconducting flux pumps. *Supercond.*, page 100022, 2022.

[7] Oomen M P, Leghissa M, Ries G, Proelss N, Neumueller H-W, Steinmeyer F, Vester M and Davies F. HTS flux pump for cryogen-free HTS magnets. *IEEE Trans. Appl. Supercond.*, 15(2):1465–1468, 2005.

[8] Hoffmann C, Pooke D and David Caplin A. Flux pump for HTS magnets. *IEEE Trans. Appl. Supercond.*, 21(3):1628–1631, 2010.

[9] Bai Z, Ding S, Li C, Li C and Yan G. A newly developed pulse-type microampere magnetic flux pump. *IEEE Trans. Appl. Supercond.*, 20(3):1667–1670, 2010.

[10] Geng J and Coombs T A. Mechanism of a high-Tc superconducting flux pump: Using alternating magnetic field to trigger flux flow. *Appl. Phys. Lett.*, 107(14):142601, 2015.

[11] Fu L, Matsuda K, Baghdadi M and Coombs T A. Linear flux pump device applied to high temperature superconducting (HTS) magnets. *IEEE Trans. Appl. Supercond.*, 25(3):1–4, 2015.

[12] Geng J and Coombs T A. An HTS flux pump operated by directly driving a superconductor into flux flow region in the E-J curve. *Supercond. Sci and Technol.*, 29(9):095004, 2016.

[13] Zhou P, Ma G, Deng Y, Nie X, Zhai Y, Liu K, Zhang H and Li Y. A contactless self-regulating HTS flux pump. *IEEE Trans. Appl. Supercond.*, 30(4):1–6, 2020.

[14] Bumby C W, Jiang Z, Storey J G, Pantoja A E and Badcock R A. Anomalous open-circuit voltage from a high-Tc superconducting dynamo. *Appl. Phys. Lett.*, 108(12):122601, 2016.

[15] Bumby C, Pantoja A, Sung H-J, Jiang Z, Kulkarni R and Badcock R. Through-wall excitation of a magnet coil by an external-rotor HTS flux pump. *IEEE Trans. Appl. Supercond.*, 26(4):1–5, 2016.

[16] Hoffmann C, Walsh R, Karrer-Mueller E and Pooke D. Design parameters for an HTS flux pump. *Phys. Procedia*, 36:1324–1329, 2012.

[17] Geng J, Painter T, Long P, Gawith J, Yang J, Ma J, Dong Q, Shen B, Li C and Coombs T A. A kilo-ampere level HTS flux pump. *Supercond. Sci and Technol.*, 32(7):074004, 2019.

[18] Zhang H, Geng J and Coombs T A. Magnetizing high-Tc superconducting coated conductor stacks using a transformer–rectifier flux pumping method. *Supercond. Sci and Technol.*, 31(10):105007, 2018.

[19] Geng J, Bumby C and Badcock R. Maximising the current output from a self-switching kA-class rectifier flux pump. *Supercond. Sci and Technol.*, 33(4):045005, 2020.

[20] Ainslie M, Grilli F, Quéval L, Pardo E, Perez-Mendez F, Mataira R, Morandi A, Ghabeli A, Bumby C and Brambilla R. A new benchmark problem for electromagnetic modelling of superconductors: The high-Tc superconducting dynamo. *Supercond. Sci and Technol.*, 33(10):105009, 2020.

[21] Mataira R, Ainslie M, Badcock R and Bumby C. Origin of the DC output voltage from a high-Tc superconducting dynamo. *Appl. Phys. Lett.*, 114(16):162601, 2019.

[22] Mataira R, Ainslie M, Badcock R and Bumby C. Modeling of stator versus magnet width effects in high-Tc superconducting dynamos. *IEEE Trans. Appl. Supercond.*, 30(4):1–6, 2020.

[23] Ainslie M, Quéval L, Mataira R and Bumby C. Modelling the frequency dependence of the open-circuit voltage of a high-Tc superconducting dynamo. *IEEE Trans. Appl. Supercond.*, 31(5):1–7, Aug. 2021.

[24] Zhou P, Ren G, Ainsile M, Ghabeli A, Zhang S, Zhai Y and Ma G. Impact of magnet number on the DC output of a dynamo-type HTS flux pump. under review.

[25] Sokolovsky V and Prigozhin L. HTS dynamo flux pump: The impact of a ferromagnetic stator substrate.

[26] Ghabeli A, Pardo E and Kapolka M. 3D modeling of a superconducting dynamo-type flux pump. *Sci. Rep*, 11(1):1–12, 2021.

[27] Geng J and Coombs T A. Modeling methodology for a HTS flux pump using a 2D H-formulation. *Supercond. Sci and Technol.*, 31(12):125015, 2018.

[28] Zhou P, Zhou Y, Ainsile M, Ghabeli A, Grilli F and Ma G. Charging process simulation of a coil by a self-regulating high-T_c superconducting flux pump. under review.

[29] Ainslie M. Numerical modelling of high-temperature superconducting dynamos: a review. *Supercond.*, page 100033, 2022.

[30] Ghabeli A, Ainslie M, Pardo E, Quéval L and Mataira R. Modeling the charging process of a coil by an HTS dynamo-type flux pump. *Supercond. Sci and Technol.*, 34(8):084002, 2021.

[31] Bai Z, Ma C, Chen C and Pang Y. Study on the excitation of a Bi-2223 small superconducting coil by a pulse-type magnetic flux pump. *IEEE Trans. Appl. Supercond.*, 27(2):1–5, 2017.

[32] Jiang Z, Hamilton K, Amemiya N, Badcock R A and Bumby C W. Dynamic resistance of a high-Tc superconducting flux pump. *Appl. Phys. Lett.*, 105(11):112601, 2014.

[33] Jiang Z, Bumby C, Badcock R, Sung H-J, Long N J and Amemiya N. Impact of flux gap upon dynamic resistance of a rotating HTS flux pump. *Supercond. Sci and Technol.*, 28(11):115008, 2015.

[34] Ghabeli A and Pardo E. Modeling of airgap influence on DC voltage generation in a dynamo-type

flux pump. *Supercond. Sci and Technol.*, 33(3):035008, 2020.

[35] Santos G D, Sass F, Sotelo G G, Fajoni F, Baldan C A and Ruppert E. Multi-objective optimization for the superconducting bias coil of a saturated iron core fault current limiter using the T-A formulation. *Supercond. Sci and Technol.*, 34(2):025012, 2021.

[36] Santos G D, Martins F G R, Sass F, Dias D H N, Sotelo G G and Morandi A. A coupling method of the superconducting devices modeled by finite element method with the lumped parameters electrical circuit. *Supercond. Sci and Technol.*, 34(4):045014, 2021.

[37] Santos G D, Santos B M O, Martins F G R, Sass F, Sotelo G G, and Andrade R. An integrated methodology to assess AC losses in the kHz range using the fem and partial element equivalent circuit. *IEEE Trans. Appl. Supercond.*, 32(2):1–8, 2021.

[38] Pardo E, Šouc J and Frolek L. Electromagnetic modelling of superconductors with a smooth current–voltage relation: variational principle and coils from a few turns to large magnets. *Supercond. Sci and Technol.*, 28(4):044003, 2015.

[39] Pardo E and Kapolka M. 3D computation of non-linear eddy currents: Variational method and superconducting cubic bulk. *J. Comput. Phys.*, 344:339 – 363, 2017.

[40] NM Strickland, C Hoffmann, and SC Wimbush. A 1 ka-class cryogen-free critical current characterization system for superconducting coated conductors. Review of Scientific Instruments, 85(11), 2014.

[41] Zhang H, Zhang M and Yuan W. An efficient 3D finite element method model based on the T-A formulation for superconducting coated conductors. *Supercond. Sci and Technol.*, 30(2):024005, 2016.

[42] Liang F, Venuturumilli S, Zhang H, Zhang M, Kvitkovic J, Pamidi S, Wang Y and Yuan W. A finite element model for simulating second generation high temperature superconducting coils/stacks with large number of turns. *J. Appl. Phys.*, 122(4):043903, 2017.

[43] Zermeno V, Abrahamsen A B, Mijatovic N, Jensen B B and Sørensen M P. Calculation of alternating current losses in stacks and coils made of second generation high temperature superconducting tapes for large scale applications. *J. Appl. Phys.*, 114(17):173901, 2013.

[44] Berrospe-Juarez E, Zermeño Víctor, Trillaud F and Grilli F. Real-time simulation of large-scale HTS systems: Multi-scale and homogeneous models using the T-A formulation. *Supercond. Sci and Technol.*, 32(6):065003, 2019.

[45] Zhou P, Santos G D, Ghabeli A, Grilli F and Ma G. Coupling electromagnetic numerical models of HTS coils to electrical circuits: multi-scale and homogeneous methodologies using the T-A formulation. *Supercond. Sci and Technol.*, 35(11):115005, 2022.